Structural Engineering and Mechanics, Vol. 32, No. 3 (2009) 447-457
DOI: http://dx.doi.org/10.12989/sem.2009.32.3.447

Analytical modeling of thin-walled box T-joints

Prabhakar R. Marur†

India Science Lab, General Motors R&D, Creator, ITP, Bangalore - 560 066, India

(Received July 28, 2008, Accepted April 30, 2009)

Abstract. A general analytical method for computing the joint stiffness from the sectional properties of the members that form the joint is derived using Vlasov's thin-walled beam theory. The analytical model of box T-joint under out-of-plane loading is investigated and validated using shell finite element results and experimental data. The analytical model of the T-joint is implemented in a beam finite element model using a revolute joint element. The out-of-plane displacement computed using the beam-joint model is compared with the corresponding shell element model. The results show close correlation between the beam revolute joint model and shell element model.

Keywords: joint flexibility; torsional distortion; revolute joint; T-joint; thin-walled beam.

1. Introduction

Automotive frames consist of closed channel sections joined together to form the body structure. Since the thin-walled channel sections are the major load carrying members, the automobile structure can be adequately modeled using one-dimensional beam elements. As the overall stiffness and dynamic behavior of the structure is of interest in the concept design stages, such beam element models are of immediate use. Computation with beam finite elements reduces the order of analysis, permits parametric study to evaluate several concept designs, and also enables optimization of body structures (Fredrickson 2003).

While beams adequately model the channel sections, the overall behavior of the automotive frames can be simulated only by accounting for the flexibility of the structural joints where the load carrying members meet. The structural joint flexibility not only affects the body stiffness but also influences the vibration and crash characteristics. Hence an important aspect in developing reduced order models using one-dimensional elements is in accounting for the flexibility at the structural joints.

Borowski *et al.* (1973) studied the influence of joint flexibility on the dynamic response characteristics of an automotive frame using experimental and numerical methods. It was found that the beam element model with rigid joints predicted lower natural frequencies that were 60 percent in error with the test results. In order to match the numerical results with the experimental data, fictitious linear springs were introduced. Chang (1974) investigated the effect of flexible connections on the structural response of a body frame under different in-plane loading conditions. The author noted that if rigid connections were used in the finite element model, the computed

† E-mail: prabhakar.marur@gm.com

deflections were only one half of the test results for the frontal loading cases.

Lubkin (1974) determined the lower vibration modes of a H-shaped research frame by treating the joint region as substructure with plate elements in a model otherwise composed of bar elements. Using static condensation, the author developed a hybrid model. The fundamental frequency predicted by the model with only bar elements was 37 percent in error with the test data, while the hybrid model predicted the frequency within seven percent of the test results.

Sakurai and Kamada (1988) analyzed the static behavior of a T-shaped joint and performed parametric study to accomplish weight reduction while maintaining necessary structural joint stiffness. El-Sayed (1989) presented a finite element formulation to calculate the torsional spring rate for any number joints using the data obtained from tests or from shell finite elements.

Choi *et al.* (1996) investigated a box channel T-joint and compared the strain energy obtained from beam and shell models. It was noted that the difference in the computed strain energy between the two models was mostly concentrated in the vicinity of the joint area. By changing the section properties for the beam elements in that region, the strain energy in the beam model was matched with the shell model. From the results of the numerical experiments, the authors concluded that torsion mode is more important than the bending mode when considering joint flexibility. Bylund (2003) devised a dynamic analysis method by placing lumped masses at the ends of the joint, and by using the eigenfrequencies and eigenmodes estimated the joint stiffness.

The available literature on automotive joints demonstrate the need for representing the joints by finite stiffness, however the existing computational techniques require either a shell element model of the joint or a physical prototype to determine the flexibility coefficients. Construction of shell models requires a complete definition of the geometry, and also the joint stiffness computed is dependent on the location where the joint is cut from the full vehicle model (Kim *et al*. 1995, Choi *et al*. 1996). Hence in the early concept design stages of the vehicle development process, a design-oriented analytical method for computing joint flexibility is desired.

In this paper, a general analytical method for computing the joint stiffness of box cross section is presented. The thin-walled theory of beams due to Vlasov (1920) is employed for computing the stiffness of T-joints under out-of-plane loading, and the computed results are compared with those obtained using shell finite elements. A simple revolute joint technique is devised to introduce joint flexibility in a beam finite element model, and the static structural response is compared with the corresponding shell element model.

2. Analysis of T-joint model

The analytical expressions derived for thin-walled beam deformations can be used for estimating the flexibility of T-joints. In this paper, a box-beam T-joint under out-of-plane loading is studied. The T-joint is formed with three equal arms, and a normal load is applied to one of the members, while the other two arms are fixed.

2.1 Analytical formulation

Consider the thin-walled box cross section shown in Fig. 1(a). The deformation of the beam under a torsional load can be computed by superposing the torsional rotation $V_\theta(z)$, section distortion $V_\chi(z)$ and warping deformation $U(z)$. Treating these deformations as the unknowns in the problem,

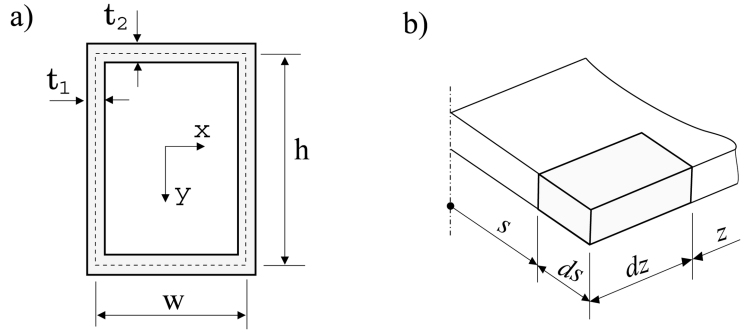

Fig. 1 a) Thin walled box-beam geometry, b) A differential element

the longitudinal displacement $u(z, s)$ and the tangential displacement $v(z, s)$ of beam cross section can be given as (Vlasov 1920)

$$u(z,s) = U(z)\varphi(s), \quad v(z,s) = V_\theta(z)\varphi_\theta(s) + V_\chi(z)\varphi_\chi(s) \tag{1}$$

where $\varphi(s)$, $\varphi_\theta(s)$ and $\varphi_\chi(s)$ are chosen functions of single argument of contour coordinate s. The generalized internal forces corresponding to longitudinal displacement, torsion, and contour distortion are B the longitudinal bimoment, H the torsional moment and Q the transverse bimoment, respectively. Applying equilibrium conditions, a system of six differential equations can be obtained and can be solved in closed form (Vlasov 1920). Since boundary conditions are known either in terms of the displacements (U, V_θ, V_χ) or in terms of the generalized forces (B, H, Q), the system of equations can be uniquely solved. The general solution is given in terms of arbitrary constants C_1 through C_6, and the products of hyperbolic functions. The details of the notation and forms of hyperbolic functions are given in Appendices A and B.

In the system of differential equations derived by Vlasov (1920), it can be shown that $H(z)$ is constant, implying that the torsion in the beam is constant regardless of the boundary conditions of the beam, and it can be given as

$$H = C_5 \frac{b_2^2 - b_1^2}{b_2} \tag{2}$$

from which C_5 is evaluated. Further, as the constant C_6 appears only in the equation for V_θ, hence the constants C_1 through C_4 can be solved simultaneously as

$$\begin{Bmatrix} U \\ V_\chi \\ B \\ Q \end{Bmatrix} = \begin{pmatrix} A_1\Phi_4 + B_1\Phi_2 & A_1\Phi_3 - B_1\Phi_1 & A_2\Phi_1 + B_2\Phi_3 & A_2\Phi_2 - B_2\Phi_4 \\ A_3\Phi_1 + B_3\Phi_3 & A_3\Phi_2 - B_3\Phi_4 & A_4\Phi_4 + B_4\Phi_2 & A_4\Phi_3 - B_4\Phi_1 \\ A_1\Phi_2 - B_1\Phi_4 & A_1\Phi_1 + B_1\Phi_3 & A_2\Phi_3 - B_2\Phi_1 & A_2\Phi_4 + B_2\Phi_2 \\ A_3\Phi_3 - B_3\Phi_1 & A_3\Phi_4 + B_3\Phi_2 & A_4\Phi_2 - B_4\Phi_4 & A_4\Phi_1 + B_4\Phi_3 \end{pmatrix} \begin{Bmatrix} C_1 \\ C_2 \\ C_3 \\ C_4 \end{Bmatrix} + \begin{Bmatrix} C_5 \\ 0 \\ 0 \\ 0 \end{Bmatrix} \tag{3}$$

and finally, C_6 can be evaluated from

$$V_\theta(z) = C_1(A_5\Phi_1 + B_5\Phi_3) + C_2(A_5\Phi_2 - B_5\Phi_4) + C_3(A_5\Phi_3 - B_5\Phi_1) + C_4(A_5\Phi_4 + B_5\Phi_2) - C_5\left(\frac{b_1}{b_2}\right)z - C_6\left(\frac{b_1}{b_2}\right) \tag{4}$$

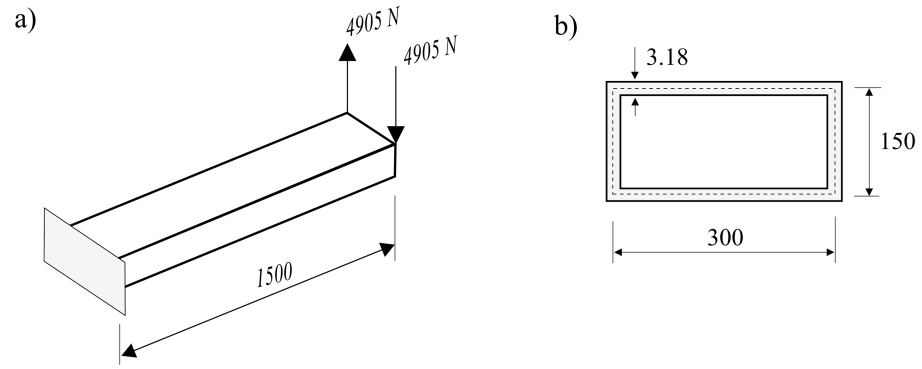

Fig. 2 Cantilever box-beam specimen with uniform wall thickness (Boswell and Zhang 1985). All dimensions are in mm

The analytical computations are compared with the test data obtained with corner loading of typical thin-walled cantilever box beam available in the literature for specific boundary conditions. The geometry of the beam and the applied loads reported by Boswell and Zhang (1985) are shown in Fig. 2. From the clamped condition at the origin, the boundary conditions are $U(0) = V_{\chi}(0) = 0$. Using these boundary conditions and the first two rows of the matrix in Eq. (3), the constants C_3 and C_4 are evaluated as

$$C_3 = -\frac{1}{A_1}(B_1 C_1 + C_5)$$

$$C_4 = -\frac{A_2}{B_2} C_2 \tag{5}$$

As noted previously, the torque is constant through the length of the beam and it is given by $H = Pw$, where P is the applied corner load. From the expression for torsion, C_5 evaluates to $(Pwb_2)/(b_2^2 - b_1^2)$.

For the applied loads, the generalized forces are given by $B(L) = 0$ and $Q(L) = Pw$. Using these boundary conditions and the expressions for C_3 through C_5 in the last two rows of the matrix in Eq. (3), a system of equations in C_1 and C_2 can be obtained as

$$\begin{Bmatrix} C_1 \\ C_2 \end{Bmatrix} = \begin{bmatrix} \left(A_3 + \frac{B_1}{A_1}B_3\right)\Phi_{1L} + \left(B_3 - \frac{B_1}{A_1}A_3\right)\Phi_{3L} & \left(A_3 - \frac{A_2}{B_2}B_3\right)\Phi_{2L} - \left(B_3 + \frac{A_2}{B_2}A_3\right)\Phi_{4L} \\ \left(A_4 + \frac{B_1}{A_1}B_4\right)\Phi_{4L} + \left(B_4 - \frac{B_1}{A_1}A_4\right)\Phi_{2L} & \left(A_4 - \frac{A_2}{B_2}B_4\right)\Phi_{3L} - \left(B_4 + \frac{A_2}{B_2}A_4\right)\Phi_{1L} \end{bmatrix}^{-1}$$

$$\begin{Bmatrix} \frac{1}{A_1}(A_3\Phi_{3L} - B_3\Phi_{1L})C_5 \\ \frac{1}{A_1}(A_4\Phi_{2L} - B_4\Phi_{4L})C_5 + Pw \end{Bmatrix} \tag{6}$$

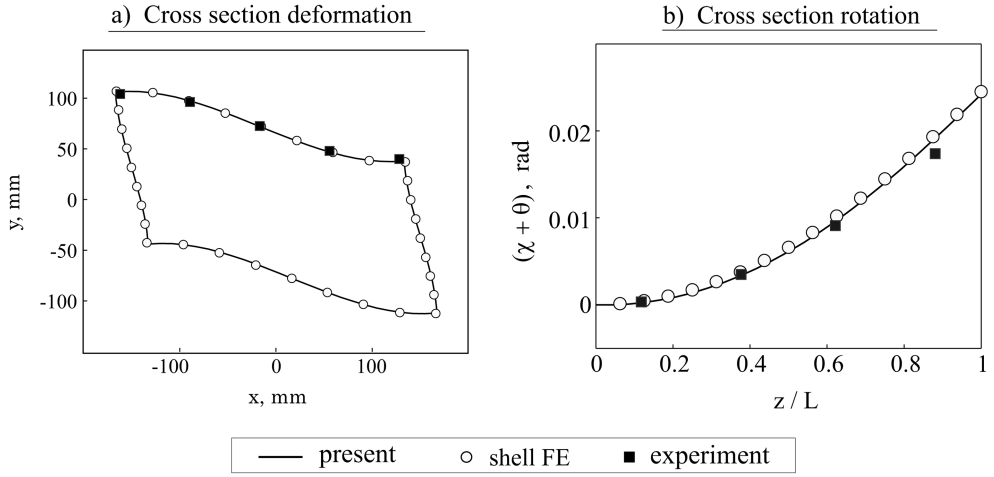

Fig. 3 a) Deformed shape of cantilever beam cross section at $z = L$, b) Distribution of longitudinal deformation and cross section rotation along the length of the beam. The experimental data are from Boswell and Zhang (1985)

where Φ_{iL} denotes Φ_i evaluated at $z = L$. Finally, the constant C_6 is obtained from the condition $V_\theta(0) = 0$ as

$$C_6 = \frac{b_2}{b_1}(C_2 A_5 + C_4 B_5) \tag{7}$$

The cross sectional deformation at $z = L$ computed using the analytical method is compared with test data in Fig. 3(a). Also shown in the figure is the numerical results obtained with shell finite element analysis. The distributions of longitudinal displacement and cross sectional distortion along the length of the beam are compared with the shell model and experimental data in Fig. 3(b). In all the cases, analytical results agree well with experimental and numerical data.

It must be noted that the derivations given in Vlasov (1920) and in this subsection are valid for rectangular cross sections only. For square cross sections, or more generally, in cases where $h/w = t_1/t_2$, the governing equations need to be rederived as shown in Appendix C.

2.2 T-Joint

In a T-joint, the arms that have fixed end conditions undergo bending in the plane perpendicular to the structure, and also torsion and section distortion about its axis. The warping deformation of these members at the joint location can be taken as zero due to the presence of the central pillar. With that assumption, the joint members can be analyzed in isolation as clamped beams with statically equivalent loading.

Since warping of the beam at the joint is taken as zero, the longitudinal reaction forces are unknown. Hence the solution presented in the previous section can be used here with one change: by using $U(L) = 0$ instead of $B(L) = 0$. The expressions for C_3 through C_6 are same as in the previous section. The constants C_1 and C_2 are obtained from solving the following equation

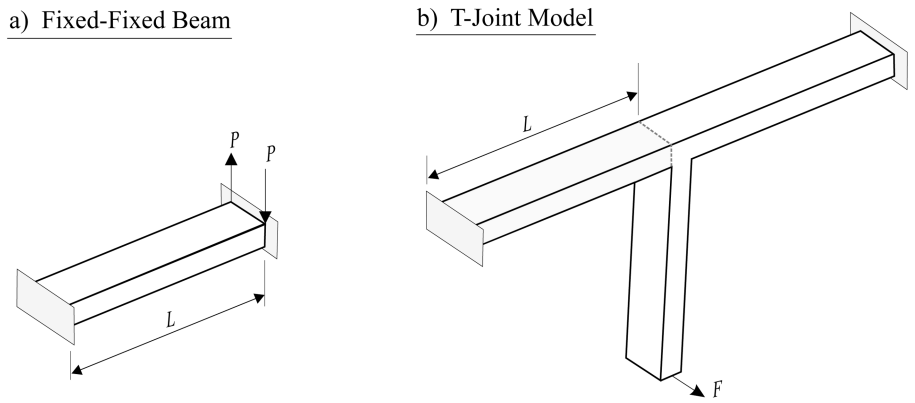

Fig. 4 a) Beam with fixed ends, b) T-joint formed using box beams

$$\begin{Bmatrix} C_1 \\ C_2 \end{Bmatrix} = \begin{bmatrix} \left(A_1 + \frac{B_1^2}{A_1}\right)\Phi_{4L} & \left(A_1 - \frac{A_2}{B_2}B_1\right)\Phi_{3L} - \left(B_1 + \frac{A_2}{B_2}A_1\right)\Phi_{1L} \\ \left(A_4 + \frac{A_1}{B_1}B_4\right)\Phi_{1L} + \left(B_4 - \frac{B_1}{A_1}A_4\right)\Phi_{2L} & \left(A_4 - \frac{A_2}{B_2}B_4\right)\Phi_{3L} - \left(B_4 + \frac{A_2}{B_2}A_4\right)\Phi_{1L} \end{bmatrix}^{-1}$$

$$\begin{Bmatrix} \left(1 - \Phi_{2L} + \frac{B_1}{A_1}\Phi_{4L}\right)C_5 \\ \left(\frac{A_4}{A_1}\Phi_{2L} - \frac{B_4}{A_1}\Phi_{4L}\right)C_5 + Pw \end{Bmatrix} \tag{8}$$

In order to validate the assumption of zero longitudinal displacement at the joint location, the box beam cantilever described in the previous section is modeled here with clamped end conditions as shown in Fig. 4(a). In addition, a T-joint is formed using the box beams for comparison as shown in Fig. 4(b); the cross section dimensions of the beams are identical to that shown in Fig. 2. The out-of-plane load F is chosen such that it induces the same corner load on the joint members as in the previous section.

The finite element mesh for the beam with fixed ends and the T-joint are constructed using 4-noded shell elements. The in-plane nodal displacements of the end cross section are extracted from the finite element results and the deformed profile of the cross section is constructed. The deformed shape of the cross section at $z = L$ is shown in Fig. 5 along with that obtained using analytical results. The theoretical computations correlate well with the results obtained from the shell model of the T-joint and the beam with fixed ends. The distributions of longitudinal deformation and cross section distortion along the length of the joint members are shown in Fig. 6. The analytical results are in close agreement with the shell element results. The displacements of the T-joint computed using the boundary condition $B(L) = 0$ instead of $U(L) = 0$ are also shown in the figure for reference.

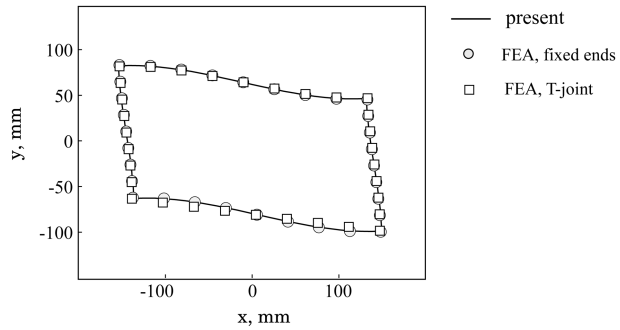

Fig. 5 Deformed shapes of the beam cross section at $z = L$

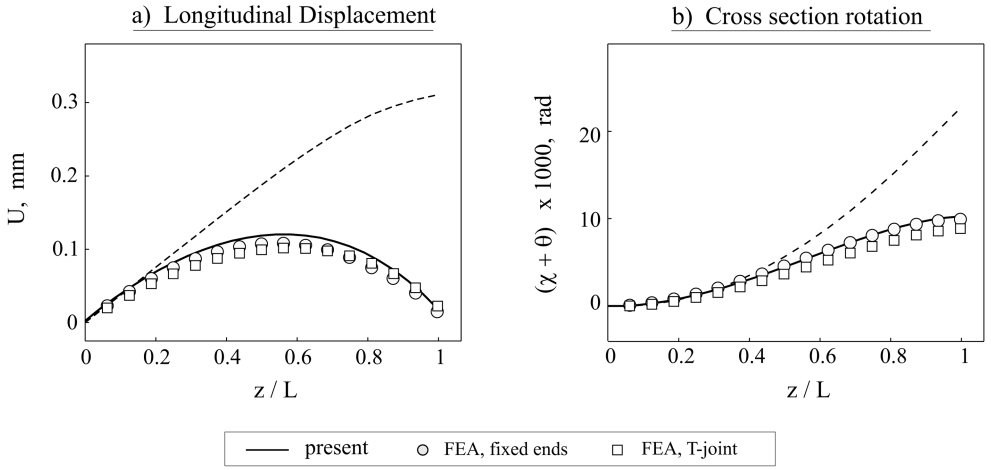

Fig. 6 Distribution of longitudinal deformation and cross section rotation along the length of the beam with fixed ends and the section of the T-joint (Dashed line represents the case $U(L) \neq 0$)

3. Beam element model

The joint flexibility can be introduced in the finite element analysis of vehicle structures in several ways. Special beam finite elements can be formulated by including extra degrees of freedom to account for the distorsional and shear effects (Zhang and Lyons 1984, Paavola 1992, Prokic 1993). The higher order elements provide an accurate representation of the thin-walled beam, but such elements cannot be directly implemented in the standard finite element packages used in the engineering analysis. A much simpler alternative would be to account for the additional deformation due to contour distortion using discrete elements such as revolute joints, linear springs, etc.

In this paper, a revolute joint element is used to account for joint flexibility in the beam model. The beams are connected through a revolute joint as shown in Fig. 7(a), with the direction of rotation along the z-axis. The rotational stiffness of the revolute joint is computed from the T-joint model presented in the previous section. A point load F is applied at the free end of the T-joint frame as shown in Fig. 7(a), and the out-of-plane displacements of the center pillar are computed using the beam joint model, and the shell element model shown in Fig. 7(b). The deflected profile

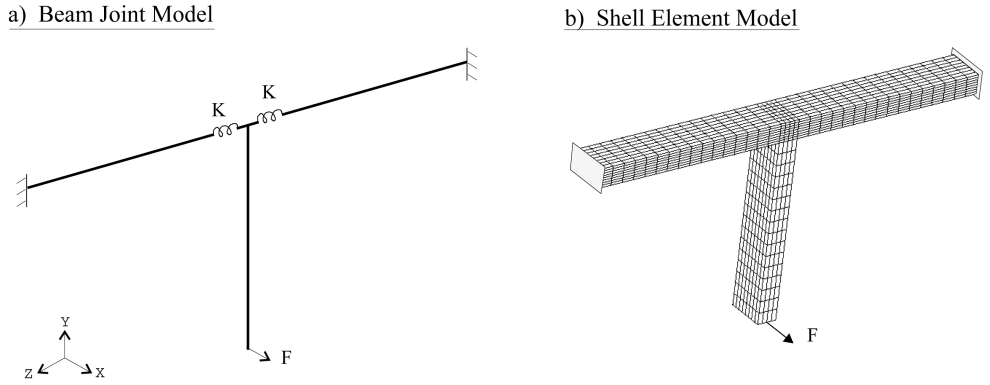

Fig. 7 Beam joint model and the corresponding shell finite element model

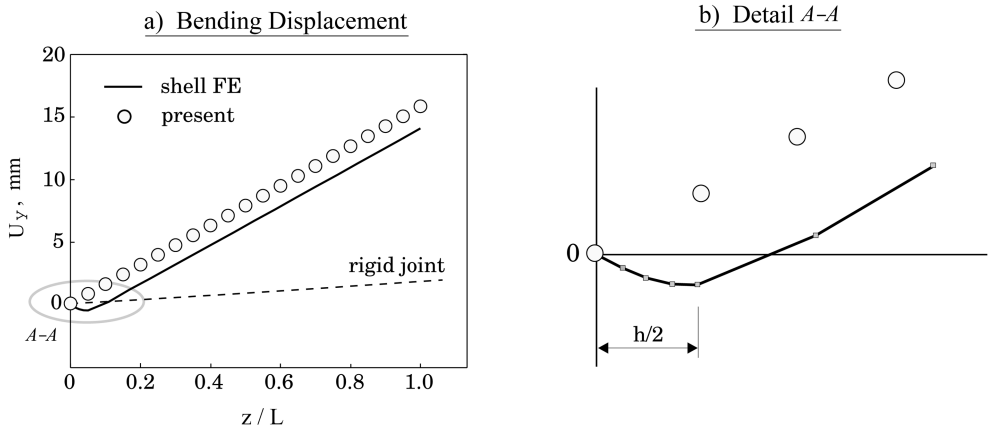

Fig. 8 Distribution of bending deflection of the center arm of the T-joint

of the free arm of the T-joint is compared with that obtained with the shell model in Fig. 8. The deflected shape of center arm obtained with rigid joint is also shown in the figure for reference. The bending deflection obtained from the beam joint model is in good agreement with the shell finite elements, albeit with a small offset. The offset is due to the deformation of the plate section from the centroid of the T-joint to the location where the joint arm originates as shown in Fig. 8(b).

4. Conclusions

Analytical expressions are derived using thin walled beam theory to estimate the joint stiffness of box beams from the cross sectional deformation of connecting members. The analytical results match well with shell finite element model and experiments at the basic beam level. The validated analytical model is employed to analyze a T-joint under out-of-plane loading. The joint flexibility is incorporated in a beam finite element model of the T-joint using revolute joint elements. The out-of-plane displacement computed using the beam model is in good agreement with that obtained using shell finite elements.

References

Borowski, V.J., Steury R.L. and Lubkin, J.L. (1973), "Finite element dynamic analysis of an automotive frame", *SAE Paper 730506*.

Boswell, L.F. and Zhang, S.H. (1985), "An experimental investigation of the behavior of thin-walled box beams", *Thin Wall. Struct.*, **3**, 35-65.

Bylund, N. (2003), "Fast and economical stiffness evaluation of mechanical joints", *SAE Paper 2003-01-2751*.

Chang, D.C. (1974), "Effects of flexible connections on body structural response", *SAE Trans.*, **83**, 233-244.

Choi, J.K., Choi, S.H., Lee, Y.R. and Lee, J.H. (1996), "A study of the beam modeling of box channel structures: for the T-type joint structures", *SAE Paper 960554*.

El-Sayed, M.E.M. (1989), "Calculation of joint spring rates using finite element formulation", *Comput. Struct.*, **33**, 977-981.

Fredricson, H.A. (2003), "Design process for property based optimization of vehicle body structures", *SAE Paper 2003-01-2755*, 2003.

Kim, Y.Y., Kang, J.H., Yim, H.J. and Kim, J.H. (1995), "Reconsideration of the joint modeling technique: In a box-beam T-joint", *SAE Paper 951108*.

Lubkin, J.L. (1974), "The flexibility of a tubular welded joint in a vehicle frame", *SAE Paper 740340*.

Paavola, J. (1992), "A finite element technique for thin-walled girders", *Comput. Struct.*, **44**, 159-175.

Prokic, A. (1993), "Thin-walled beams with open and closed cross-sections", *Comput. Struct.*, **47**, 1065-1070.

Sakurai, T., and Kamada, Y. (1988), "Structural joint stiffness of automotive body", *SAE Paper 880550*.

Vlasov, V.Z. (1961), *Thin-walled Elastic Beams*, The Israel Program for Scientific Translations: Jerusalem.

Zhang, S.H. and Lyons, L.P.R. (1984), "A thin-walled box beam finite element for curved bridge analysis", *Comput. Struct.*, **18**, 1035-1046.

Appendix A. Notation

h : height of beam cross section
s : contour coordinate
t : thickness
u : longitudinal displacement
v : tangential displacement
w : width of beam cross section
z : length coordinate
B : longitudinal bimoment
E : Young's modulus
F : transverse load
G : Shear modulus
H : torsional moment
J : moment of inertia
L : beam length
M : bending moment
P : corner load
Q : transverse bimoment
U : warping function
V_θ : section rotation function
V_χ : distortion function
θ : torsion angle
φ : generalized warping coordinate
ψ_θ : generalized torsion coordinate
ψ_χ : generalized distortion coordinate

Appendix B. Joint parameters

The hyperbolic functions used in Section 2.1 are given by

$$\Phi_1(z) = \cosh(\alpha z)\sin(\beta z); \quad \Phi_2(z) = \cosh(\alpha z)\cos(\beta z);$$
$$\Phi_3(z) = \sinh(\alpha z)\cos(\beta z); \quad \Phi_4(z) = \sinh(\alpha z)\sin(\beta z); \tag{B.1}$$

where α and β are the real part and the imaginary part of the four conjugate complex roots of the characteristic equation of the differential equation.

The coefficients A_1 through A_5, and B_1 through B_5 are given by

$$\begin{aligned} A_1 &= \alpha, & B_1 &= \beta \\ A_2 &= (\alpha^4 - 6\alpha^2\beta^2 + \beta^4)/n^4, & B_2 &= 4\alpha\beta(\alpha^4 - \beta^2)/n^4 \\ A_3 &= -am^2, & B_3 &= -2a\alpha\beta \\ A_4 &= a\alpha(\alpha^2 - 3\beta^2), & B_4 &= a\beta(3\alpha^2 - \beta^2) \\ A_5 &= -2(m^2/n^4)(b_2/b_1)m^2, & B_5 &= -4(m^2/n^4)(b_2/b_1)\alpha\beta \end{aligned} \tag{B.2}$$

The parameters m and n are given by

$$m^2 = \frac{b_1 c}{2(b_1^2 - b_2^2)}, \quad n^4 = \frac{c}{a} \tag{B.3}$$

The geometric parameters are given by

$$\begin{aligned} a &= \frac{E}{24}h^2w^2(ht_1 + wt_2), & b_1 &= \frac{G}{2}hw(ht_2 + wt_1) \\ b_2 &= \frac{G}{2}hw(-ht_2 + wt_1), & c &= \frac{96E}{\frac{h}{J_1} + \frac{w}{J_2}} \end{aligned} \tag{B.4}$$

where $J_i = t_i^3/12$, $i = 1, 2$, correspond to the moments of inertia per unit length of the side of the cross section; E and G are Young's modulus and shear modulus respectively.

Appendix C. Beams with square cross section

In the case of square cross sections, or more generally, in the case where $h/w = t_1/t_2$, the coefficient b_2 is zero. Hence the coupled differential equations for the special case are given by

$$\begin{aligned} aU'' - b_1U - b_1V_\chi' &= 0 \\ b_1V_\theta'' &= 0 \\ b_1U' + b_1V_\chi'' - cV_\chi &= 0 \end{aligned} \tag{C.1}$$

By virtue of Eq. $(C.1)_2$, the longitudinal variation of angle of rotation has to be linear and it can be given as

$$V_\theta(z) = C_5z + C_6 \tag{C.2}$$

The first expression in Eq. (C.1) is identically zero for the new function $g(z)$ if the following equations are satisfied

$$\begin{aligned} U &= g' \\ V_\chi &= \frac{a}{b_1} g'' - g \end{aligned} \tag{C.3}$$

where the functional term (z) is dropped for clarity. The internal forces can be given in terms of the new function as

$$\begin{aligned} B &= -ag'' \\ H &= b_1 C_5 \\ Q &= ag''' \end{aligned} \tag{C.4}$$

Substitution of Eq. (C.3) into Eq. $(C.1)_3$ leads to the differential equation,

$$g^{IV} - \frac{c}{b_1} g'' + \frac{c}{a} g = 0 \tag{C.5}$$

which can be put in the following form

$$g^{IV} - 2m^2 g'' + n^4 g = 0 \tag{C.6}$$

The general solution of the differential Eq. (C.6) can be obtained as

$$g(z) = \sum_{i=1}^{4} C_i \Phi_i(z) \tag{C.7}$$

Eq. $(C.4)_2$ shows that the torsion is constant regardless of the end conditions and it can be used to evaluate C_5. From the boundary conditions of the problem and Eq. (C.2), C_6 can be determined. The constants C_1 through C_4 can be determined from

$$\begin{Bmatrix} U \\ V_\chi \\ B \\ Q \end{Bmatrix} = \begin{pmatrix} A_1\Phi_4 + B_1\Phi_2 & A_1\Phi_3 - B_1\Phi_1 & A_1\Phi_2 - B_1\Phi_4 & A_1\Phi_1 + B_1\Phi_3 \\ A_2\Phi_1 + B_2\Phi_3 & A_2\Phi_2 - B_2\Phi_4 & A_2\Phi_3 - B_2\Phi_1 & A_2\Phi_4 + B_2\Phi_2 \\ A_3\Phi_1 + B_3\Phi_3 & A_3\Phi_2 - B_3\Phi_4 & A_3\Phi_3 - B_3\Phi_1 & A_3\Phi_4 + B_3\Phi_2 \\ A_4\Phi_4 + B_4\Phi_2 & A_4\Phi_3 - B_4\Phi_1 & A_4\Phi_2 - B_4\Phi_4 & A_4\Phi_1 + B_4\Phi_3 \end{pmatrix} \begin{Bmatrix} C_1 \\ C_2 \\ C_3 \\ C_4 \end{Bmatrix} \tag{C.8}$$

where

$$\begin{aligned} A_1 &= \alpha, & B_1 &= \beta \\ A_2 &= \frac{am^2}{b_1} - 1, & B_2 &= \frac{a}{b_1}(2\alpha\beta) \\ A_3 &= -am^2, & B_3 &= -2a\alpha\beta \\ A_4 &= a\alpha(\alpha^2 - 3\beta^2), & B_4 &= a\beta(3\alpha^2 - \beta^2) \end{aligned} \tag{C.9}$$